Acta Geophysica
vol. 62 no. 3 pp. 1-18
DOI: 10.2478/s11600-013-00

FEM × DEM modelling of cohesive granular materials: numerical homogenisation and multi-scale simulation

Trung Kien NGUYEN,[1] Gaël COMBE,[1]
Denis CAILLERIE,[1] and Jacques DESRUES[1]

[1]UJF-Grenoble 1, Grenoble-INP, CNRS UMR5521,
3SR Lab., B.P.53, 38041 Grenoble Cedex 09,
France, e-mail: jacques.desrues@3sr-grenoble.fr

Abstract

This article presents a multi-scale modelling approach of cohesive granular materials, its numerical implementation and its results. At microscopic level, a Discrete Element Method (DEM) is used to model dense grains packing. At the macroscopic level, the numerical solution is obtained by a Finite Element Method (FEM). In order to bridge the micro and macro scales, the concept of Representative Elementary Volume (REV) is applied, in which the average REV stress and the consistent tangent operators are obtained in each macroscopic integration point as the results of DEM's simulation. In this way, the numerical constitutive law is determined through the detailed modelling of the microstructure, therefore taking into account the nature of granular materials. We first elaborate the principle of the computation homogenisation (FEM × DEM), then demonstrate the features of our multi-scale computation in terms of a biaxial compression test. Macroscopic strain localization is observed and discussed.

Key words: Multi-scale, FEM, DEM, homogenisation, cohesive granular materials.

1. INTRODUCTION

Numerical modelling is widely used to investigate geophysical and geotechnical problems. The Finite Element Method (FEM) (Zienkiewicz 1979), which is based on a continuum approach, can be applied. This method is appropriate for a wide range of applications (cliff stability, soil mechanics, etc.). For example, earth structures specifically made of granular materials are very common (Chevalier *et al.* 2011). Granular media are discontinuous and heterogeneous by nature. Such materials generate complex mechanical responses when subjected to small (Atman 2009) as well as large deformations (Lanier 2001, Szarf 2011). Unfortunately, it is difficult to realistically model the discrete nature of granular matter by FEM. Conversely, the Discrete Discrete Element Methods (DEM) has been especially developed to model the granular materials at the particle scale. This numerical method consists in taking into account contacts between rigid bodies and in integrating the equations of motion for each grain to obtain the response of an assembly of particles (Cundall and Strack 1979). The granular media is modelled at the contact scale and then, their discrete nature is captured.

It is known that the mechanical behaviour of granular soils take its origins at the grain scale (inter-granular contact behaviour, contact network and its evolution, packing fraction, ...) hereafter called the *microstructure*. The mathematical and the numerical description of a two-scale relationship between the microstructure and the macroscopic mechanical behaviour is an essential issue. Recently, several authors have proposed multi-scale approach with various strategies. On one hand, Feyel and Chaboche (2000), Kouznetsova *et al.* (2001, 2002) and Feyel (2003) suggest to model the behaviour of the microstructure *via* a FEM approach, coupled with another FEM modeling at the macroscale. This technics is known as a FEM^2 approach. On the other hand, some other authors develop strategies to build mechanical equivalent laws with DEM numerical modeling of the microstructure, Miehe and Dettmar (2003), Meier *et al.* (2007) and Miehe *et al.* (2010).

In this paper, we propose a new multi-scale numerical homogenisation approach by closely combining FEM and DEM to study the behaviour of cohesive granular materials. The microstructure of the granular soil is modelled by using the DEM approach on a Representative Elementary Volume (REV) made of few grains. At the large scale (earth structure), the FEM approach is used. In this way, the overall earth structure is modelled by a FEM approach. The constitutive mechanical behaviour used at each integration points of the mesh comes from the behaviour computed with DEM of a REV and not from a mathematically formulated phenomenological law. The micro (DEM) and the macro (FEM) scales are bridged by a numerical homogenisation process described hereafter in the paper.

In fact, due to friction, the behaviour of granular media is essentially non-elastic, and strain history dependent which means that the stress at some instant depend not only on the strain at that instant but on the whole history of strain up to it. The boundary value problems (BVP) involving solids presenting such a behaviour are therefore evolution problems. Very often, those evolu-

tions are slow enough so that inertial effects can be neglected and the evolution is quasi-static which means that at any time the medium is in equilibrium. The numerical resolution of this type of problem is usually performed using a time stepping discretisation. In this method, the equilibrium equations are written at each time step, and the constitutive law is integrated through a specific method adapted to the law (see for instance Simo and Hughes (1998) for elastoplasticity). That yields an "integrated" constitutive equation: $\varepsilon_n \rightarrow \sigma_n$ giving the stress at the end of the step n in terms of the strain at the end of the same step and therefore looking like an elastic, generally non linear, constitutive equation.
The problem to be solved at time step n is a nonlinear elastic-like equilibrium problem, generally solved using the Newton's method. The standard Newton's method requires the differentiation of the integrated law which leads to the notion of consistent tangent operator (for elastoplasticity, see Simo and Hughes (1998)).
In the FEM $\times$ DEM approach, the macroscopic constitutive equation of the equivalent continuous granular medium is obtained through the DEM simulation of the motion of the grains in a REV subjected to a history of macroscopic strain. The integrated law of each time step is then directly the constitutive equation of the continuous medium for a macroscopic strain path completely determined by the strain at the end of the step. In this case, the numerical differentiation, which seems to be the only way to get the consistent tangent operator of the integrated law on a time step, may pose problems in some cases. Then, a variant of Newton's method is used, either by keeping the linear operator of all the time step and all the iterations equal to the elastic one of initial REV or by computing at each iteration of the Newton's method of a given time step the homogenized linear elastic constitutive equation of the current REV, the set of contacts between grains of which has been fixed.
The paper is organized as follows. Section 2 presents the homogenisation methods to bridge the scale between micro- and macro- level. Section 3 describes the numerical model by DEM. Some numerical results obtained with the multi-scale computation (FEM $\times$ DEM) is demonstrated in section 4.

2. HOMOGENISATION METHOD

The framework of multi-scale coupling method is described in Fig.1. At the macroscopic level, a quasi-static finite strain continuum formulation is considered. The resolution of BVP through FEM requires a consitutive law at each integration point of the mesh which expresses the stress (σ_{ij}) as a function of the history of displacement gradient (h_{kl}) as follow:

$$\sigma_{ij}(t) = \Gamma^t\{h_{kl}(\tau), \tau \in (0,t)\} \tag{1}$$

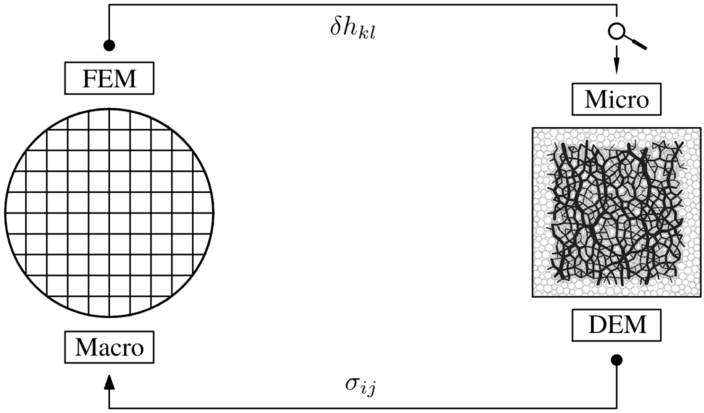

Fig.1 Computational homogenisation scheme (Nguyen *et al.* 2013)

In order to capture the main effects of granular materials, a numerical homogenisation method by DEM computation is used to build the constitutive law. In this way, for a given history of macroscopic displacement gradient h_{kl}, the macroscopic Cauchy stress σ_{ij} results from microscopic forces between grains through a well etablished homogenisation formula (Weber 1966):

$$\sigma_{ij} = \frac{1}{S} \cdot \sum_{(n,m)\in C} \vec{f}^{\,m/n} \otimes \vec{r}^{\,nm} \tag{2}$$

Where S in 2D case is the area of the microstructure; $\vec{f}^{\,m/n}$ and $\vec{r}^{\,nm}$ are respectively the contact forces acting in contact $c = (n, m)$ and the branch vector $\vec{r}^{\,nm}$ joining the mass centre of two grains (n, m) in contact.
The numerical integration of constitutive law requires to solving a nonlinear system of equations when the mechanical behaviour is nonlinear which is the case for granular materials. In order to solve the non-linear system of equations, an incremental-iterative strategy Newton-Raphson method is adopted. This requires the implementation of a consistent tangent matrix in the numerical integration scheme as defined in the equation eq.(3):

$$C_{ijkl} = \frac{d\sigma_{ij}}{dh_{kl}} \tag{3}$$

Then, the consistent tangent operators computed from the stress state at the end of the load step are consistent with the algorithm of integration used. Any inconsistency between the tangent operator and the algorithm of integration of the constitutive law will spoil the quadratic convergence of the Newton-Raphson method. Moreover, the more this operator represents the mechanical behaviour of granular media, the faster the iterative process converges to the solution.

The consistent tangent operators can be found analytically for simple laws, but for more complex laws, a numerical differentiation has to be adopted. We describe here this numerical procedure: the consistent tangent operator is evaluated in two steps.
For an increment of displacement gradient δh_{kl}, we perform a first step in which we compute the stress at the end of this increment, noted $\sigma_{ij}(\delta h_{kl})$. Then we consider perturbed increments of displacement gradient $\delta h_{kl} + \epsilon \cdot \Delta_{kl}^{mn}$. Here ϵ is a small parameter and Δ_{kl}^{mn} is a second-order tensor such that its components are defined as:

$$\Delta_{kl}^{mn} = \delta_{mk} \cdot \delta_{nl} \tag{4}$$

with the Kronecker symbol $\delta_{mk} = \begin{cases} 1 & \text{if} \quad m = k \\ 0 & \text{if} \quad m \neq k \end{cases}$. In two dimensional case: $k, l, m, n = 1, 2$.
Finally, the results of these two steps allow for the determination of consistent tangent operator:

$$C_{ijkl} = \frac{\sigma_{ij}(\delta h_{kl} + \epsilon \cdot \Delta_{kl}^{mn}) - \sigma_{ij}(\delta h_{kl})}{\epsilon} \tag{5}$$

This procedure is performed in every time step and in every Gauss point of the macroscopic finite element discretization. At the beginning and the end of each step, the REV is in a state of equilibrium.

3. MICROSCOPIC DEM MODEL

The numerical approach used to model the REV of granular material is the Discrete Element Method (DEM) using bi-Periodic Boundary Conditions (PBC) (for details see Radjai and Dubois 2011). The REV of grains is a dense packing of 400 polydisperse circular 2D particles in which grains radii are uniformly distributed between R_{min} and R_{max} such that $R_{max}/R_{min} = 5/2$, Fig. 2(a).
All grains interact via linear elastic laws and Coulomb friction when they are in contact. The normal repulsive contact force f_{el} is related to the normal apparent interpenetration δ (Fig. 2(b)) in the contact as $f_{el} = -k_n \cdot \delta$, where k_n is a normal stiffness coefficient ($\delta < 0$ if a contact is present, $\delta = 0$ if there is no contact). In order to model a cohesive material, a local cohesion is introduced for each contact by adding an attractive force f_c to f_{el}; $f_c < 0$ is here chosen constant for each pair of particles in contact. Thus, the overall normal force in a contact is $f_n = f_{el} + f_c$. A degradation of the cohesion is taken into account by considering a vanishing of f_c when a contact separation occurs. If a new contact is created during the deformation process of the REV, then the local cohesion remains nil (un-recoverable cohesion). That give “fragility property” to the assembly of grains such that it models brittle materials.

The tangential contact force f_t results from an accumulation of increments $\Delta f_t = k_t \cdot \Delta u_t$ computed at each time step (Δu_t is the tangential relative displacement in the contact and k_t is the corresponding tangential stiffness). The Coulomb condition is considered using the following inequality $|f_t| \leq \mu \cdot f_{el}$, which leads to some amount of slip (Cundall and Strack 1979).

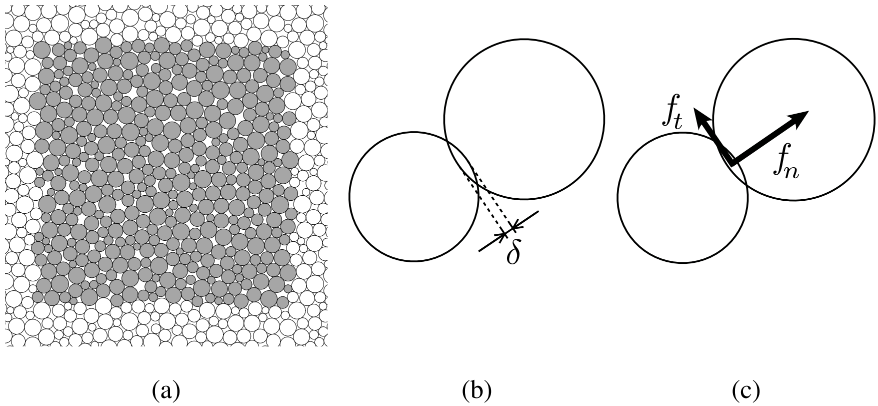

Fig.2 (a) Assembly of 400 particles (grey discs) submitted to an isotropic pressure σ_0. White grains in (a) are images of the grey discs to illustrate the bi-periodic boundary conditions. Contact between two grains: (b) overlapping δ between discs, (c) normal f_n and f_t tangential contact forces.

The numerical/mechanical parameters need by DEM require specific values. In the present study, k_n is such that the rigidity level κ defined by Combe et Roux (2003) is $\kappa = k_n/\sigma_0 = 1000$, where σ_0 is the 2D confining pressure. k_t is choosen like the stiffness ratio is $k_n/k_t = 1$. The cohesive force f_c is defined with reference to the confining pressure as suggested by Gilabert *et al.* (2007): $p^* = f_c/(a \cdot \sigma_0)$ where a is typical diameter of grains. So p^* is a ratio measuring the attractive part of a contact force versus the repulsive part due to particle interpenetration. Hereafter $p^* = 1$. The inter-granular angle of friction is $\mu = 0.5$. All parameters are summarized in table 1.
The contact friction and the contact cohesion give macroscopic mechanical failure properties to the REV, *i.e.*, an internal angle of friction φ and an overall cohesion C. To evaluate these two mechanical parameters at the REV scale, one way is to perform a "pure" DEM computation of a mechanical test like a *Biaxial* test (vertical compression with an imposed vertical constant strain rate $\dot{\varepsilon}_1$ and a constant lateral stress $\sigma_2 = \sigma_0$). Thus, a biaxial test is performed on a REV in which each contact is initially cohesive. $\dot{\varepsilon}_1$ is chosen such that the strain process of the REV can be considered as a quasi-static process (Inertial number $I < 10^{-4}$; Radjaï & Dubois 2011). The evolution of the strength of the REV and its volumetric evolution are shown on Fig. 3(a). One can notice

Table 1 Microscopic parameters

	Parameter	Value
$\kappa = k_n/\sigma_0$	Stiffness number	1000
k_n/k_t	Stiffness ratio	1
μ	Intergranular friction coefficient	0.5
p^*	Cohesion number	1

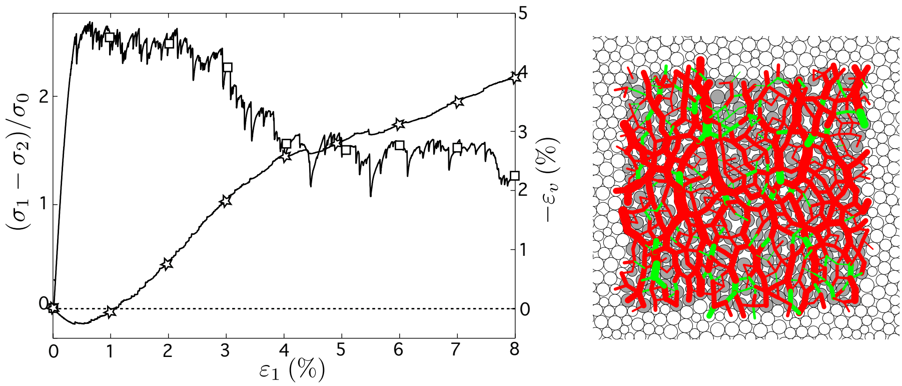

(a) (b)

Fig.3 Biaxial test (vertical compression) computed by means of DEM on a REV of 400 particles: (a) Mechanical response of the REV. The curve with the square symbols is the evolution of the deviatoric stress normalized by the confining pressure $(\sigma_1 - \sigma_2)/\sigma_0$ with the vertical strain ε_1. The curve with the star symbols is the evolution of the volumic strain ($\varepsilon_v = tr\ (\varepsilon)$) with the vertical strain. (b) REV deformed, $\varepsilon_1 = 3\%$. Contact forces are displayed with the following convention: the width of the lines joining the centres of two particles in contact is proportional to the normal force. Red and green lines distinguish respectively ($f_c \neq 0$) and ($f_c = 0$).

that whereas the lateral stress is kept constant during the vertical compression ($\sigma_2 = \sigma_0$), the vertical deviatoric stress $\sigma_1 - \sigma_2$ reaches a peak for $\varepsilon \simeq 0.6\%$ and decreases to a plateau ($\varepsilon > 4\%$). Concerning the volumetric strain ε_v, one can observe that the REV is essentially dilative (soil convention is used, $\varepsilon > 0$ for compression).

The Mohr – Coulomb failure criterion is widely applied for cohesive granular materials. With this criterion, the maximum strength is ruled by the Coulomb equation $\tau = \sigma_n \tan\varphi + C$, with two phenomenological intrinsic parameters: a macroscopic cohesion parameter C and an internal friction angle φ. In the following, these parameters are determined with two biaxial tests: one in compression (see Fig. 3(a) for the associated stress evolution) and another one in extension (stress evolution not shown in this paper). Furthermore, depending on the strain level ε_1, two set of mechanical parameters are measured: $\{\varphi, C/\sigma_0\}_p$ for the maximum strength ($\varepsilon \simeq 0.6\%$) and $\{\varphi, C/\sigma_0\}_t$ for large strains ($\varepsilon > 4\%$). The corresponding stress states are shown with Mohr circles on the Fig. 4. At the stress peak ($\varepsilon \simeq 0.6\%$), circles I and II gives $\{\varphi, C/\sigma_0\}_p = \{25^o, C/\sigma_0 = 0.3\}$ (Fig. 4(a)). When $\varepsilon > 4\%$, one should notice the vanishing of macroscopic cohesion $\{\varphi, C/\sigma_0\}_t = \{25^o, C = 0\}$ (circles III and IV on Fig. 4(b)). This last observation is related to the unrecoverability of the cohesion at the contact scale. One may notice that the angle of friction φ does not depend on the strain level.

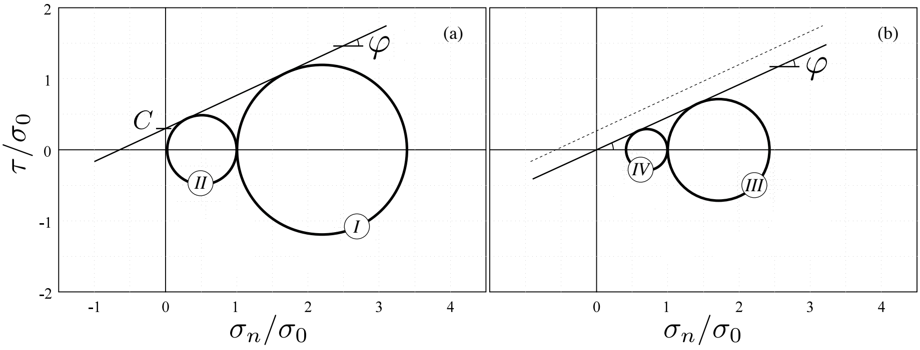

Fig.4 Mohr – Coulomb analysis of two biaxial tests. Circles I and III correspond to two stress states for biaxial test in compression. Circles II and IV show two stress states during the biaxial test in extension. Circles I and II correspond to the stress state for the maximum strength, for the two biaxial tests. Circles III and IV show the stress state for large strains, in the two biaxial tests. Bold lines shows the Coulomb criterion failure, with friction and cohesion on the left and only friction on the right, the one on the left recalled the one on the right figure with a dashed line.

4. MULTISCALE FEM × DEM SIMULATION

The FEM × DEM approach was implemented in the FEM code Lagamine (Charlier 1987) which is able to manage finite strains. The implementation involved significant modification in the original code, but it essentially consisted in adding the DEM modelling as a constitutive numerical law.

To highlight the capabilities of this new FEM×DEM approach, we present hereafter a two-scale modeling of a Biaxial vertical compression test. The granular

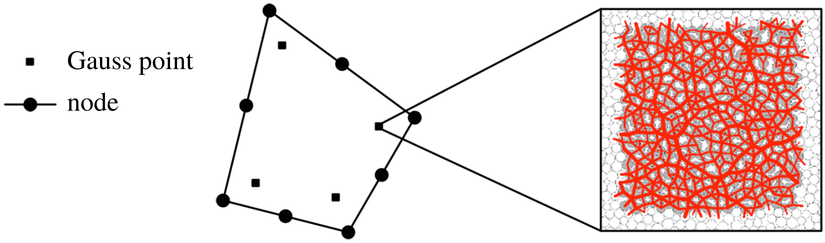

Fig.5 Q8 Element and the REV associated to each Gauss point to obtain the numerical behaviour law. The REV is submitted to an isotropic loading : all normal contact forces f_n are positives ($f_n = f_c + f_{el} > 0$) and every contact is cohesive ($f_c < 0$, $|f_c| < f_{el}$).

sample is spatially discretized using a continuum mech made of Q8 elements (8 nodes per element, 4 Gauss points per element, Fig. 5). As in some experiments (Desrues (1984), Desrues and Viggiani (2004)), the sample has initially an aspect ratio of 2. At the boundaries of the mesh, specific kinematic and static conditions are chosen (see Fig. 6 and its caption for details). These conditions are identical to those used, for example, in some 2D experiments (Richefeu *et al.* 2012).

At micro-scale – at the Gauss points – a REV of 400 particles (chosen identical for each Gauss point at the start of the modelling, although different REV may be considered as well without adding complexity in the computation) is used. In this REV, the contact laws between particles are those detailed before. At the start of the FEM×DEM simulation, the external loading exerted on the FE mesh is isotropic. Thus, going down to the micro-scale, in each Gauss point, the REV is isotropically loaded and all contacts are compressive but with adhesion (Fig. 5).

4.1. Macroscopic results

The mechanical strength evolutions of the granular material simulated via the FEM × DEM approach and with "pure" DEM are shown on the Fig. 7. This figure shows the deviatoric stress $q = \sigma_1 - \sigma_2$ normalized by σ_2 as a function of axial deformation ε_1.

The first remark is that this mechanical behaviour is typical of what is classically observed with a laboratory drained triaxial test on dense cemented sands, or weak sandstones: from the isotropic state ($q = 0$), the deviatoric stress q increases until it reaches a peak corresponding to the maximum strength of the material (hardening phase). It is remarkable that whatever the numerical method used (FEM×DEM with different meshes, pure DEM with differ-

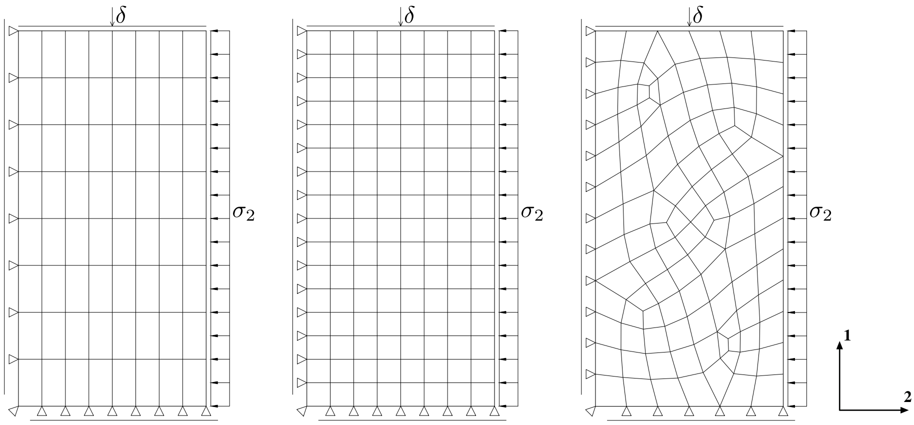

a. FD64: FEM×DEM with 64 Q8 elements

b. FD128: FEM×DEM with 128 Q8 elements

c. FD106: FEM×DEM with 106 Q8 elements

Fig.6 Spatial discretization of the granular soil for the FEM×DEM modeling. Three kind of mesh are tested: (a,b) structural mesh and (c) non-structural mesh. The vertical Biaxial compression uses identical boundary conditions for (a), (b) and (c). On the right of the mesh, we apply a constant lateral stress $\sigma_2 = \sigma_0$. On the top, an increment of displacement δ is imposed. On the left, nodes can vertically move without friction. Finally, on the bottom of the mesh, an horizontal "lubrication" is applied because nodes can only move horizontally. On may notice that the node on the left-bottom, in blocked.

ent grain numbers), the hardening phase is observed to be almost the same ($\varepsilon < 0.3\%$). Afterward, one can see a softening behaviour (stress drops down) until q reach a plateau in the FEM×DEM simulation as well as for "pure" DEM computations as soon as the number of particles is large enough ($\geq$ 22500). This softening is observed to be "computational method dependent" i.e. the post-peak response depends on the details of the method used; however, for each numerical approach (FEMxDEM on one hand, pure DEM on the other hand), the final parts of the different curves seem to tend to a unique for each numerical approach, seems to converge to a unique curve when the number of elements is increased (number of Q8 for the FEM×DEM and number of particles for "pure" DEM). This is consistent with previous research works by Chambon *et al.* (1998) and Matsushima *et al.* (2002).
The softening (post-peak response of the specimen, $0.6\% < \varepsilon < 3.5\%$) observed with FEM×DEM is more pronounced if compared with purely DEM computation for one main and *important* reason: strain localisation. Not surprisingly, strain localisation occurs in the multi-scale FEM × DEM approach. In Fig.8 (a, b, c), the local distortion of the mesh shows clearly a shear band in

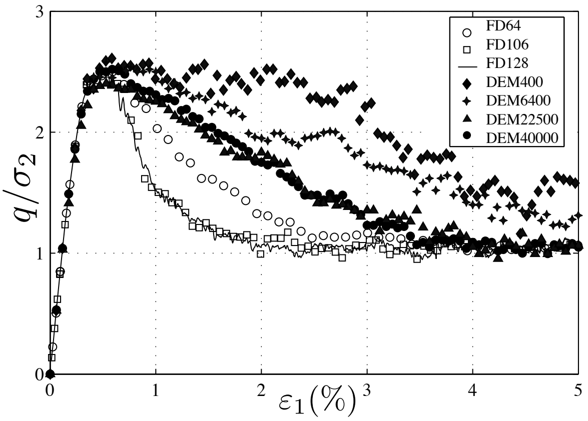

Fig.7 Macroscopic response of multi-scale FEM $\times$ DEM computations (bold line and white symbols) and "pure" DEM (black symbols) for a vertical Biaxial compression. FDxxx denotes FEM$\times$DEM computations with xxx

the specimen, confirmed on the Fig.8 (d, e, f) by the map of the deviatoric strain ($\varepsilon_D = \varepsilon_I - \varepsilon_{II}$). Due to strain localisation, deformation is concentrated in this narrow zones (called *shear band*) (Desrues and Chambon 2002) ; a given increment of top boundary displacement is no more accommodated by an overall strain in the whole specimen, but by a much faster shear deformation process in the band. In experimental tests, localisation occurs as well (Bésuelle *et al.* (2000), Desrues and Viggiani (2004)), and the seek for a proper modeling of strain localisation has been a crucial research objective for three decades now.
For FEM$\times$DEM, the peak stress can be associated to a "sudden" localisation of the strains into a shear band. However, whereas FD106 and FD128 q vs. ε_1–curves are almost superposed, FD64 softening phase is different probably because of Q8 shapes used (see Fig. 6) that constraints more (geometrically) the shear band.
Shear bands are also observed in "pure" DEM computation. Strains do not localizes "suddenly", they develop gradually, as already observed by Szarf *et al.* (2011). Fig. 9 shows maps of the second invariant of the strain tensor in samples of difference sizes, for $\varepsilon_1 = 5\%$. Whereas the REV of 400 grains do not show shear banding, strain localisation in bands can be seen in samples with 6400 particles. These shear bands are even more obvious in the DEM computation on sample of 22500 and 40000 particles. One may notice that even if Periodic Boundary Conditions are used in "pure" DEM computations, not only the localisation of deformation is observed. One may notice that, despite Periodic Boundary Conditions computations, still localisation of deformation

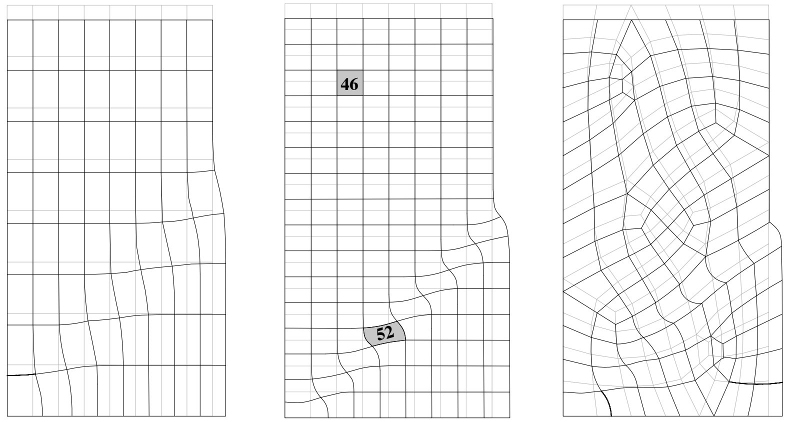

a. FD64 b. FD128 c. FD106

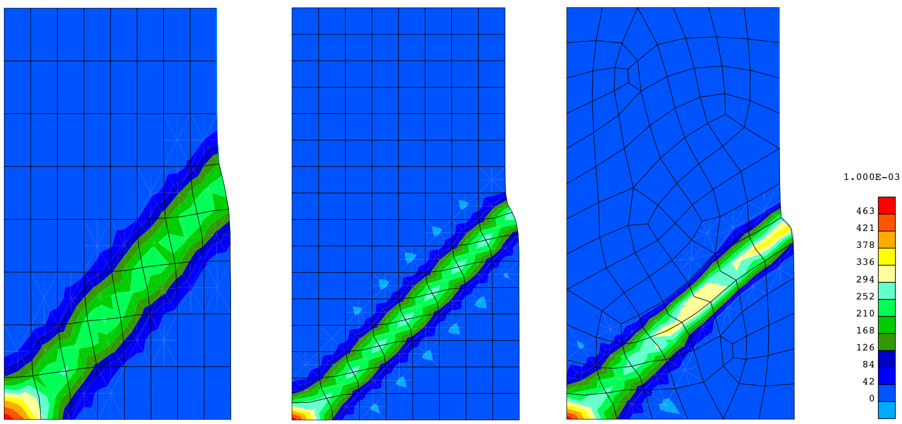

d. FD64 e. FD128 f. FD106

Fig.8 (a, b, c): maps of the initial and the deformed mesh (top), (d, e, f): maps of second invariant of strain tensor when $\varepsilon_1 = 3\%$. (bottom).

is observed; however, the resulting shear bands have to respect the periodicity condition, which is an artificial and non realistic constraint on shear band patterns. For this reason, no attempt is made to use microscopic shear band orientation in an upscaling process toward the macroscopic scale.

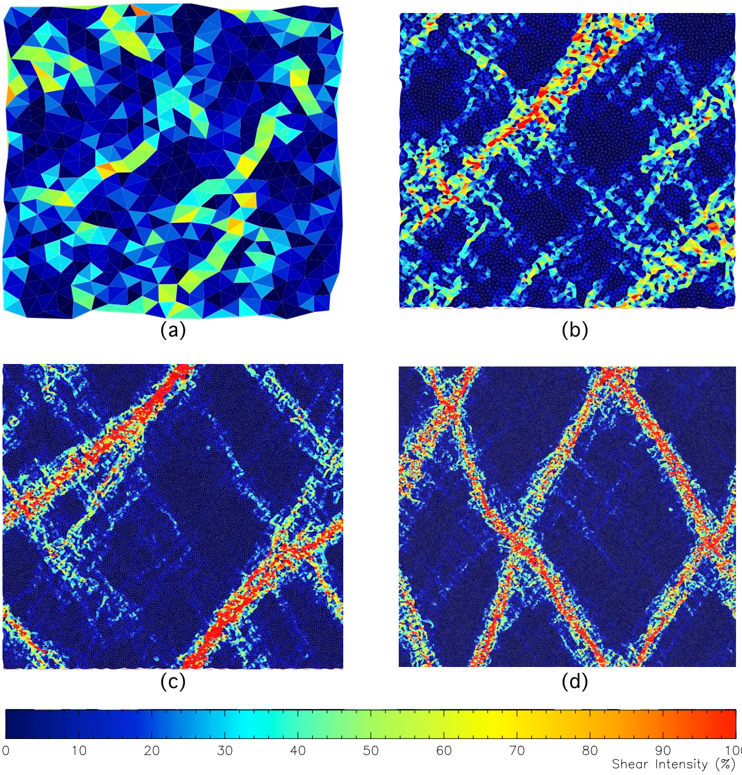

Fig.9 Maps of the local second invariant of the total strain tensor ε_D (shear intensity) computed on sample of (a) 400, (b) 6400, (c) 22500 and (d) 40000 particles submitted to a biaxial loading. $\varepsilon_1 = 5\%$. Local ε_D is computed for triplet of grains (Delaunay triangulation), using the approach suggested by Calvetti *et al.* (1997).

4.2. Microscopic analysis

In order to highlight the advantage of our methods and to understand the origin of macroscopic phenomena, which comes from the microscopic evolution, in this section, we propose to analyze the stress evolution in various Gauss points at different location in the mesh. The mesh of 128 elements Q8 is chosen for this analysis. The focus is on the Gauss points into Q8 n^o 46 and Q8 n^o 52 (see Fig.8b). The element 52 is located in the shear band whereas the element 46 is far from the shear band, in a homogeneous zone.

Fig.10 shows the evolution of principal stresses (PS hereafter) (minor and major) in the two elements. As for the major PS, we observe that their respective evolutions diverge once the maximum shear strength is reached. The stress variations are rather smooth in element 46 and noisy in 52. Both 46 and 52

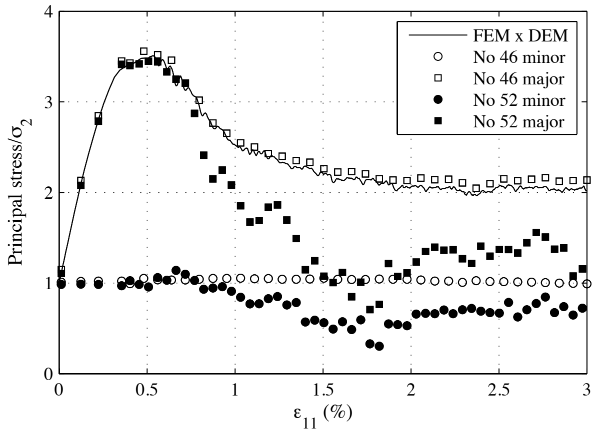

Fig.10 Microscopic analysis: Principal stress in elements 46 and 52 (ε_{11} is the equivalent overall axial strain for the specimen).

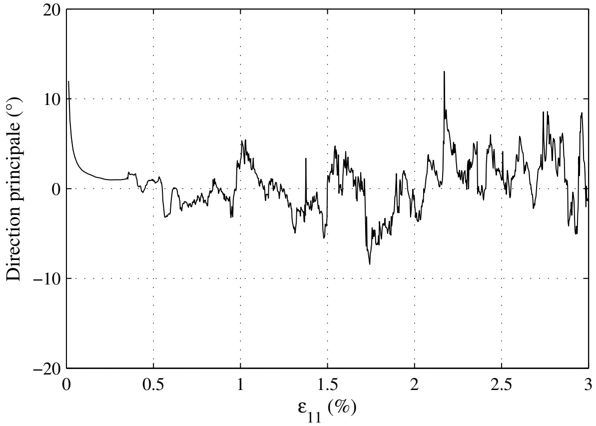

Fig.11 Microscopic analysis: Principal direction in element 52 (ε_{11} is the equivalent overall axial strain for the specimen).

show stress reduction, which is consistent with the softening of the specimen as a structure: despite the degradation of the material's properties is concentrated in the shear band, it results in a fall of stress in the whole specimen as soon as the band becomes the overall failure mechanism. The minor PS shows the same trend with respect to smoothness. Within the shear band, not only PS values but also PS directions (Fig.11) show some scatter in time. Clearly, the shear band becomes the only active part of the specimen once localisation has

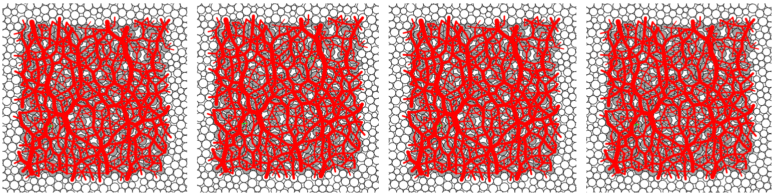

a. Gauss 1 b. Gauss 2 c. Gauss 3 d. Gauss 4

Fig.12 REV deformed at Gauss point of element 46 at global specimen strain $\varepsilon_{11} = 3\%$. (See Fig.3(b) for color convention).

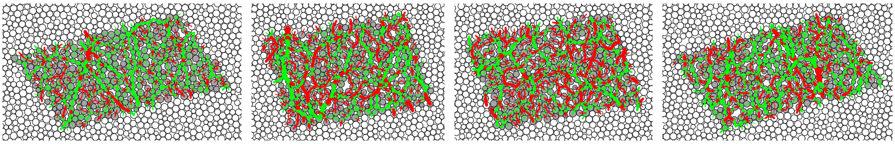

a. Gauss 1 b. Gauss 2 c. Gauss 3 d. Gauss 4

Fig.13 REV deformed at Gauss point of element 52 at global specimen strain $\varepsilon_{11} = 3\%$. (See Fig.3(b) for color convention).

started; in this active zone, the deformation process is intensive and produces large micro-structural reorganization with severe scattering in the local stress. In Fig.12 and Fig.13, the REV at deformed state are plotted. All the Gauss point have the same initial configuration (Fig.5) but the deformed configurations in the different Gauss points become different as the deformation progresses, and quite different at the end of the test, especially within the shear band. All the REV in the element 46 remain similar to the initial state with only one or two contact losing cohesion, while the REV in the element 52 is subjected to a complex loading at each REV (both compression and shear loading, see the shape of REV) while a degradation of cohesion forces is observed throughout these REV (contacts without cohesion are illustrated by the green line). We can conclude that in the shear band zone, the strain localisation leads to a generalized inter-granular cracking.

5. CONCLUSION

A multi-scale approach to investigate the behaviour of cohesive granular materials has been presented, combining DEM at the micro level with FEM modelling at macroscopic level. A numerical homogenisation method is used to bridge the gap between different scales. At small scale level, kinematics condition is applied at each REV with PBC. The mean stress is recovered together with the consistent tangent operators to construct the macroscopic constitutive law. This new method allows us to obtain the overall behaviour of geomaterials together with the micro mechanism inside REV at every point in the FEM mesh. The DEM code has been successfully implemented in a large strain finite elements code Lagamine. Using this numerical tool, some results from biaxial test simulation were presented and analyzed. Strain localisation has been observed. The mechanical response of cohesive granular materials was investigated both at the macro- and microscopic level. Moreover, local stress evolutions, and the intergranular cracking at micro level (REV) have been highlighted to understand the origin of the macroscopic behaviour.

Acknowledgments. This work was carried out as a part of GeoBridge project research at 3SR Lab, Grenoble, France (contract number: ANR-09-BLAN-0096). The authors would like to thank the French National Research Agency (ANR - Agence Nationale de la Recherche) for this support.

References

Atman, A.P.F., Claudin, P. and Combe, G. (2009), Departure from elasticity in granular layers: Investigation of a crossover overload force, *Computer Physics Communication* **180(4)**, 612-615.

Bésuelle, P., Desrues, J. and Raynaud, S. (2000), Experimental characterisation of the localisation phenomenon inside a vosges sandstone in a triaxial cell, *Journal of Rock Mechanics and Mining Sciences* **37**, 1223-1237.

Chambon, R., Caillerie, D. and El Hassan, N. (1998), One dimensional localization studied with a second grade model, *European Journal of Mechanics and Solids* **17**, 637-656.

Charlier, R. (1987), Approche unifiée de quelques problèmes non linéaires de mécanique des milieux continus par la méthode des éléments finis, *Phd thesis, University of Liège*.

Chevalier, B., Villard, P., Combe, G. (2011), Investigation of load-transfer mechanisms in geotechnical earth structures with thin fill platforms reinforced by rigid inclusions, *International Journal of Geomechanics* **11(3)**, 239-250.

Calvetti, F., Combe, G., Lanier, J. (1997) Experimental micromechanical analysis of a 2D granular material : relation between structure evolution and loading path, *Mechanics of Cohesive Frictional Materials* **2(2)**, 121-163.

Combe, G. and Roux, J.-N. (2003), Discrete numerical simulation, a quasistatic deformation and the origin of strain in granular materials, 3^{rd} *Internaltional Symposium on Deformation Characteristics of Geomaterials*, Lyon-France, 1070-1078.

Cundall, P.A. and Strack, O.D.L. (1979), A discrete numerical model for granular assemblies, *Geotechnique* **29(1)**, 47-65.

Desrues, J. (1984), La localisation de la déformation dans les matériaux granulaires. Thèse de Doctorat es Science, USMG and INPG, Grenoble, France.

Desrues, J. and Chambon, R. (2002), Shear band analysis and shear moduli calibration, *International Journalof Solids and Structures* **39**, 3757-3776.

Desrues, J. and Viggiani, G. (2004), Strain localization in sand: an overview of the experimental results obtained in Grenoble using stereophotogrammetry, *Int. J. Numer. Anal. Meth. Geomech.* **28**, 279-321.

Feyel, F. and Chaboche, J.-L. (2000), FE^2 multiscale approach for modelling the elastoviscoplastic behaviour of long fibre SiC/Ti composite materials, *Comput. Methods. Appl. Mech. Engrg* **183**, 309-330.

Feyel, F.(2003), A multilevel finite element method (FE^2) to describe the response of highly non-linear structures using generalized continua, *Comput. Methods. Appl. Mech. Engrg* **190**, 3233-3244.

Gilabert, F.A., Roux, J.-N. and Castellanos, A. (2007), Computer simulation of model cohesive powders: Influence of assembling procedure and contact laws on low consolidation states, *Physical Review E* **75**, 011303(1-26).

Kouznetsova, V., Brekelmans, W.A.M. and Baaijens, F.P.T. (2001), An approach to micro-macro modelling of heterogeneous materials, *Computational Mechanics* **27**, 37-48.

Kouznetsova, V., Geers, M.D.G. and Brekelmans, W.A.M. (2002), Multiscale constitutive modelling of heterogeneous materials with a gradient-enhanced computational homogenization scheme, *Int. J. Numer. Meth. Engnr.* **54**, 1235-1260.

Lagamine code, *University of Liège*.

Lanier, J. (2001), Mécanique des milieux granulaires, *Hermes science publications*.

Matsushima, T., Chambon, R. , Caillerie, D. (2002), Large strain finite element analysis of a local second gradient model: application to localization, *Int. J. Numer. Meth. Engnr* **54**,499-521.

Meier, H.A., Steinmann, P. and Kuhl, E. (2007), Towards multiscale computation of confined granular media, *Technische Mechanik* **28(1)**, 32-42.

Miehe, C. and Dettmar, J. (2003), A framework for micro-macro transitions in periodic particle aggregates of granular materials, *Comput. Methods Appl. Mech. Engrg.* **196**, 225-256.

Miehe, C., Dettmar, J. and Zäh, D. (2010), Homogenization and two-zcale simulations of granular materials for different microstructural constraints, *Int. J. Numer. Meth. Engnr* **83**, 1206-1236.

Nguyen, T.K., Combe, G. , Caillerie, D. and Desrues, J. (2013), Modeling of a cohesive granular materials by a multi-scale approach, *AIP Conference Proceedings* **1542**, 1194-1198.

Radjai, F. and Dubois, F. (2011), Discrete modelling of Granular Materials, *John Wiley & Son*.

Richefeu, V., Combe, G., Viggiani, G. (2012), An experimental assessment of displacement fluctuations in a 2D granular material subjected to shear, *Géotechnique Letters* **2**, 113-118.

Simo, J.C. and Hughes, T.J.R. (1998), Computational Inelasticity, *Springer*.
Szarf, K., Combe, G. and Villard, P. (2011), Polygons vs. clumps of discs: a numerical study of the influence of grain shape on the mechanical behaviour of granular materials, *Powder Technology* **208(2)**, 279-288.
Weber, J. (1966), Recherches concernant les contraintes intergranulaires dans les milieux pulvérulents, *Bul. liaison P. et Ch. No. Juillet-août*.
Zienkiewicz, O.C. (1979), La méthode des éléments finis, *Mc Graw-Hill Inc.*

Received receive date
Accepted accept date